T. L. Usher,[2] A. J. van der Horst,[40] L. Vigiani,[7] N. Vilchez,[46] V. Vitale,[49,62] A. von Kienlin,[19] A. P. Waite,[2] D. A. Williams,[4] C. Wilson-Hodge,[40] B. L. Winer,[17] K. S. Wood,[1] X. F. Wu,[26,63,64] R. Yamazaki,[41] T. Ylinen,[5,16,65] M. Ziegler[4]

[1]Space Science Division, Naval Research Laboratory, Washington, DC 20375, USA. [2]W. W. Hansen Experimental Physics Laboratory, Kavli Institute for Particle Astrophysics and Cosmology, Department of Physics and SLAC National Accelerator Laboratory, Stanford University, Stanford, CA 94305, USA. [3]Department of Physics, Tokyo Institute of Technology, Meguro City, Tokyo 152-8551, Japan. [4]Santa Cruz Institute for Particle Physics, Department of Physics, and Department of Astronomy and Astrophysics, University of California at Santa Cruz, Santa Cruz, CA 95064, USA. [5]The Oskar Klein Centre for Cosmo Particle Physics, AlbaNova, SE-106 91 Stockholm, Sweden. [6]Department of Astronomy, Stockholm University, SE-106 91 Stockholm, Sweden. [7]Istituto Nazionale di Fisica Nucleare, Sezione di Pisa, I-56127 Pisa, Italy. [8]Laboratoire AIM, CEA-IRFU/CNRS/Université Paris Diderot, Service d'Astrophysique, CEA Saclay, 91191 Gif sur Yvette, France. [9]Center for Research and Exploration in Space Science and Technology (CRESST), NASA Goddard Space Flight Center, Greenbelt, MD 20771, USA. [10]National Aeronautics and Space Administration (NASA) Goddard Space Flight Center, Greenbelt, MD 20771, USA. [11]Istituto Nazionale di Fisica Nucleare, Sezione di Trieste, I-34127 Trieste, Italy. [12]Dipartimento di Fisica, Università di Trieste, I-34127 Trieste, Italy. [13]Department of Physics and Astronomy, Rice University, MS-108, Post Office Box 1892, Houston, TX 77251, USA. [14]Istituto Nazionale di Fisica Nucleare, Sezione di Padova, I-35131 Padova, Italy. [15]Dipartimento di Fisica "G. Galilei," Università di Padova, I-35131 Padova, Italy. [16]Department of Physics, Royal Institute of Technology (KTH), AlbaNova, SE-106 91 Stockholm, Sweden. [17]Department of Physics, Center for Cosmology and Astro-Particle Physics, The Ohio State University, Columbus, OH 43210, USA. [18]University of Alabama in Huntsville, Huntsville, AL 35899, USA. [19]Max-Planck Institut für Extraterrestrische Physik, 85748 Garching, Germany. [20]Laboratoire Leprince-Ringuet, École Polytechnique, CNRS/IN2P3, Palaiseau, France. [21]Istituto Nazionale di Fisica Nucleare, Sezione di Perugia, I-06123 Perugia, Italy. [22]Dipartimento di Fisica, Università degli Studi di Perugia, I-06123 Perugia, Italy. [23]Dipartimento di Fisica "M. Merlin," dell'Università ed il Politecnico di Bari, I-70126 Bari, Italy. [24]Istituto Nazionale di Fisica Nucleare, Sezione di Bari, 70126 Bari, Italy. [25]Department of Physics, University of Washington, Seattle, WA 98195-1560, USA. [26]Pennsylvania State University, 525 Davey Laboratory, University Park, PA 16802, USA. [27]INAF (Istituto di Astrofisica Spaziale e Fisica Cosmica), I-20133 Milano, Italy. [28]Scuola Internazionale Superiore di Studi Avanzati (SISSA), 34014 Trieste, Italy. [29]George Mason University, Fairfax, VA 22030, USA. [30]Laboratoire de Physique Théorique et Astroparticules, Université Montpellier 2, CNRS/IN2P3, 34095 Montpellier, France. [31]Department of Physics and Astronomy, Sonoma State University, Rohnert Park, CA 94928-3609, USA. [32]Department of Physics, Stockholm University, AlbaNova, SE-106 91 Stockholm, Sweden. [33]Agenzia Spaziale Italiana (ASI) Science Data Center, I-00044 Frascati (Roma), Italy. [34]Stellar Solutions Incorporated, 250 Cambridge Avenue, Suite 204, Palo Alto, CA 94306, USA. [35]Dipartimento di Fisica, Università di Udine and Istituto Nazionale di Fisica Nucleare, Sezione di Trieste, Gruppo Collegato di Udine, I-33100 Udine, Italy. [36]Los Alamos National Laboratory, Los Alamos, NM 87545, USA. [37]CNRS/IN2P3, Centre d'Études Nucléaires Bordeaux Gradignan, UMR 5797, Gradignan, 33175, France. [38]Université de Bordeaux, Centre d'Études Nucléaires Bordeaux Gradignan, UMR 5797, Gradignan, 33175, France. [39]Department of Physics and Astronomy, University of Leicester, Leicester, LE1 7RH, UK. [40]NASA Marshall Space Flight Center, Huntsville, AL 35805, USA. [41]Department of Physical Science and Hiroshima Astrophysical Science Center, Hiroshima University, Higashi-Hiroshima 739-8526, Japan. [42]University of Maryland, College Park, MD 20742, USA. [43]Centre for Astrophysics Research, University of Hertfordshire, College Lane, Hatfield AL10 9AB, UK. [44]European Organization for Nuclear Research (CERN), CH-1211 Geneva, Switzerland. [45]Cosmic Radiation Laboratory, Institute of Physical and Chemical Research (RIKEN), Wako, Saitama 351-0198, Japan. [46]Centre d'Étude Spatiale des Rayonnements, CNRS/UPS, BP 44346, F-30128 Toulouse Cedex 4, France. [47]Orbital Network Engineering, 10670 North Tantau Avenue, Cupertino, CA 95014, USA. [48]University College Dublin, Belfield, Dublin 4, Ireland. [49]Istituto Nazionale di Fisica Nucleare, Sezione di Roma "Tor Vergata," I-00133 Roma, Italy. [50]Department of Physics and Astronomy, University of Denver, Denver, CO 80208, USA. [51]Institute of Space and Astronautical Science, Japan Aerospace Exploration Agency (JAXA), 3-1-1 Yoshinodai, Sagamihara, Kanagawa 229-8510, Japan. [52]Department of Physics, Graduate School of Science, University of Tokyo, 7-3-1 Hongo, Bunkyo-ku, Tokyo 113-0033, Japan. [53]University of California Observatories/Lick Observatories, Santa Cruz, CA 95064, USA. [54]Institut de Ciencies de l'Espai (IEEC-CSIC), Campus UAB, 08193 Barcelona, Spain. [55]Kavli Institute for Cosmological Physics, University of Chicago, Chicago, IL 60637, USA. [56]Space Sciences Division, NASA Ames Research Center, Moffett Field, CA 94035-1000, USA. [57]NYCB Real-Time Computing Incorporated, Lattingtown, NY 11560-1025, USA. [58]Department of Chemistry and Physics, Purdue University Calumet, Hammond, IN 46323-2094, USA. [59]INAF Osservatorio Astronomico di Brera, I-23807 Merate, Italy. [60]Institució Catalana de Recerca i Estudis Avançats (ICREA), 08010 Barcelona, Spain. [61]Consorzio Interuniversitario per la Fisica Spaziale (CIFS), I-10133 Torino, Italy. [62]Dipartimento di Fisica, Università di Roma "Tor Vergata," I-00133 Roma, Italy. [63]Joint Center for Particle Nuclear Physics and Cosmology (J-CPNPC), Nanjing 210093, China. [64]Purple Mountain Observatory, Chinese Academy of Sciences, Nanjing 210008, China. [65]School of Pure and Applied Natural Sciences, University of Kalmar, SE-391 82 Kalmar, Sweden.

*To whom correspondence should be addressed. E-mail: michael.briggs@nasa.gov (M.S.B.); htajima@slac.stanford.edu (H.T.); charles.dermer@nrl.navy.mil (C.C.D.).
†Present address: Sterrenkundig Instituut "Anton Pannekoek," 1098 SJ Amsterdam, Netherlands.

Comprehensive Characterization of Genes Required for Protein Folding in the Endoplasmic Reticulum

Martin C. Jonikas,[1,2,3,4] Sean R. Collins,[1,3,4] Vladimir Denic,[1,3,4]* Eugene Oh,[1,3,4] Erin M. Quan,[1,3,4] Volker Schmid,[5] Jimena Weibezahn,[1,3,4] Blanche Schwappach,[5] Peter Walter,[2,3] Jonathan S. Weissman,[1,3,4]† Maya Schuldiner[1,3,4]‡

Protein folding in the endoplasmic reticulum is a complex process whose malfunction is implicated in disease and aging. By using the cell's endogenous sensor (the unfolded protein response), we identified several hundred yeast genes with roles in endoplasmic reticulum folding and systematically characterized their functional interdependencies by measuring unfolded protein response levels in double mutants. This strategy revealed multiple conserved factors critical for endoplasmic reticulum folding, including an intimate dependence on the later secretory pathway, a previously uncharacterized six-protein transmembrane complex, and a co-chaperone complex that delivers tail-anchored proteins to their membrane insertion machinery. The use of a quantitative reporter in a comprehensive screen followed by systematic analysis of genetic dependencies should be broadly applicable to functional dissection of complex cellular processes from yeast to human.

The endoplasmic reticulum (ER) is responsible for the folding and maturation of secreted and membrane proteins. External stress or mutations can compromise ER folding, contributing to diseases such as diabetes and neurodegeneration (1, 2). The specialized milieu of the ER is composed of a large number of proteins that aid the structural maturation of itinerant proteins (3, 4). Although many of these ER folding factors have been extensively studied, the full range of proteins contributing to this process is unknown, and how they function together is poorly understood.

Systematic identification of genes contributing to ER folding. We exploited the cell's endogenous sensor of ER protein folding status, Ire1p, to identify genes in *Saccharomyces cerevisiae* that contribute to structural maturation of secretory proteins. In response to misfolded proteins in the ER, the transmembrane sensor Ire1p activates the transcription factor Hac1p (5), which in turn transcriptionally up-regulates a distinct set of genes (6, 7) in a process called the unfolded protein response (UPR). We used a reporter system in which a Hac1p-responsive promoter drives green fluorescent protein (GFP) expression (8) (Fig. 1A). To correct for nonspecific expression changes, we coexpressed a red fluorescent protein (RFP) from a constitutive *TEF2* promoter and used the ratio of GFP/RFP as our reporter of UPR signaling. A titration of the ER stress-inducing reducing agent dithiothreitol (DTT) demonstrated that this reporter quantitatively responds to misfolding of ER proteins (Fig. 1B).

With use of synthetic genetic array methodology (9), we introduced the reporter into ~4500 strains from the *S. cerevisiae* deletion library (10),

[1]Department of Cellular and Molecular Pharmacology, University of California, San Francisco, San Francisco, CA 94143, USA. [2]Department of Biochemistry and Biophysics, University of California, San Francisco, CA 94143, USA. [3]Howard Hughes Medical Institute, University of California, San Francisco, CA 94143, USA. [4]California Institute for Quantitative Biomedical Research, San Francisco, CA 94143, USA. [5]Faculty of Life Sciences, University of Manchester, Manchester M13 9PT, UK.

*Present address: Department of Molecular and Cellular Biology, Harvard University, Cambridge, MA 02138, USA.
†To whom correspondence should be addressed. E-mail: weissman@cmp.ucsf.edu
‡Present address: Department of Molecular Genetics, Weizmann Institute of Science, Rehovot 76100, Israel.

and the median single-cell fluorescence of each strain was measured by using high-throughput flow cytometry (*11*, *12*) (fig. S1 and table S1). The

UPR showed significant basal induction, which allowed us to identify genes whose deletion caused either up-regulation (399 hits with $P < 0.01$, ex-

plicitly modeling our experimental error) or down-regulation (334 hits with $P < 0.01$) of the reporter. We found limited overlap between the genes
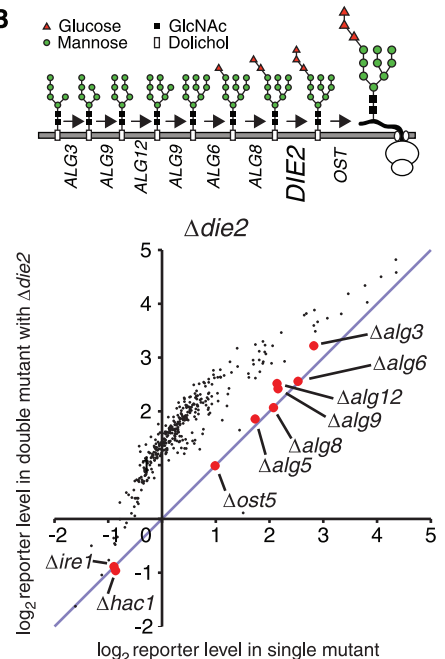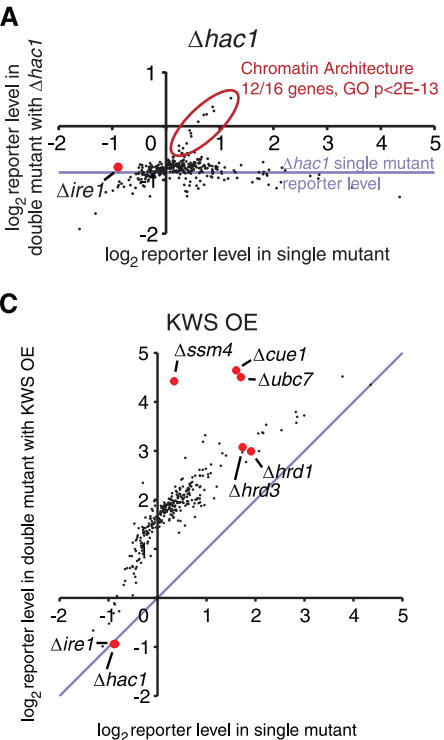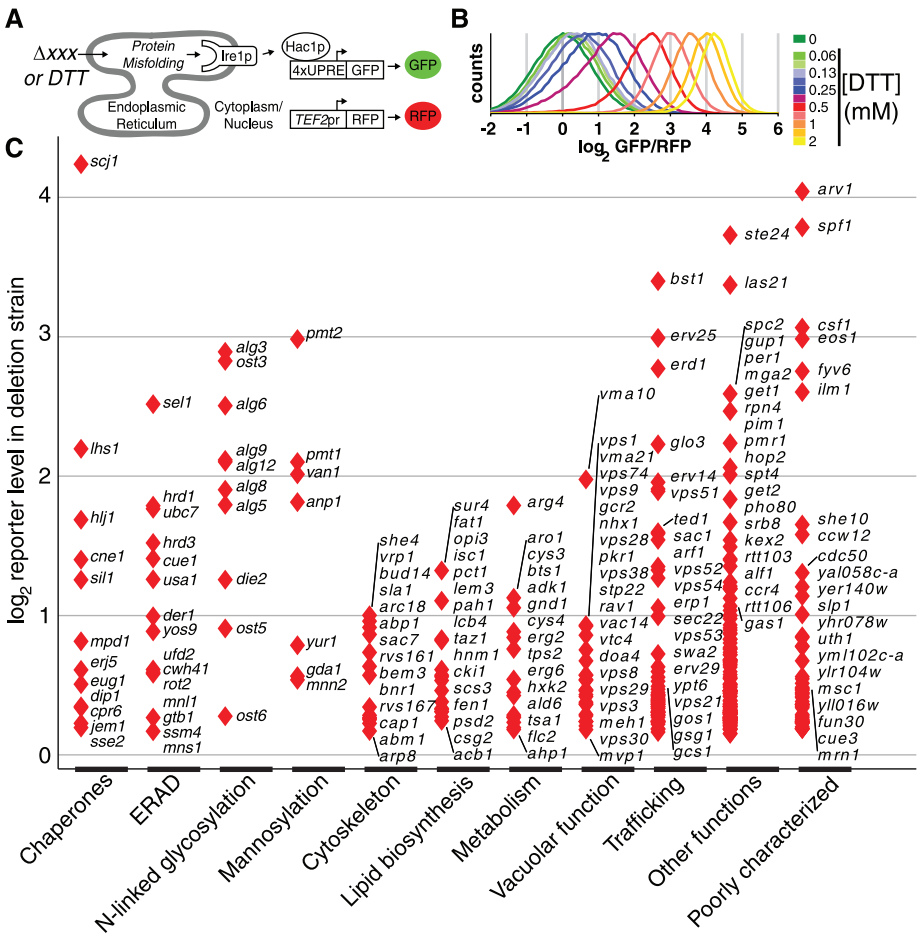
Fig. 1. Quantitative screen for gene deletions that perturb UPR signaling. (**A**) Strategy for quantifying UPR levels in deletion strains. (**B**) GFP/RFP reporter ratios as a function of concentration of DTT, a reducing agent that causes protein misfolding in the ER. (**C**) UPR reporter levels of up-regulator hits by functional category.

Fig. 2. Double mutant analysis provides information on functional dependencies between genes. (**A**) Double mutant (DM) plot of Δ*hac1*. Each point represents a gene. *X* coordinate represents the reporter level of a strain deleted for that gene in a wild-type (WT) background. *Y* coordinate represents the reporter level in a double mutant lacking the same gene and additionally deleted for a second gene (in this case, *HAC1*). The horizontal blue line indicates the reporter level in the Δ*hac1* single mutant. Circled in red are up-regulators whose reporter induction is *HAC1*-independent, which are highly enriched for chromatin architecture factors. (**B**) (Top) Schematic of the lumenal steps of the N-linked glycan synthesis pathway. (Bottom) DM plot for Δ*die2*/*alg10*. (**C**) DM plot depicting genetic interactions between deletion mutants and over-expression (OE) of the ERAD substrate KWS.

whose deletion induces the UPR and the genes that were previously shown by microarray analysis to be transcriptionally up-regulated by the UPR (7) [fig. S2 and table S2; see also (10, 13)]. Thus, although defining the UPR targets was fundamental to our understanding of how cells respond to ER stress, it provides a limited view of the processes constitutively required for folding in the ER.

Overview of gene deletions affecting the UPR. Proteins whose deletion caused up-regulation of the reporter were highly enriched for localization throughout the secretory pathway (fig. S3 and table S3) (14), including the ER as well as the Golgi, vacuole, and endosome. As expected, chaperones (15) and genes in the N-linked glycosylation (16) and ER-associated degradation (ERAD) (17) pathways featured among the top hits (Fig. 1C). However, deletion of genes involved in many other processes, including O-mannosylation, glycophosphatidylinositol anchor synthesis, lipid biosynthesis, multiple steps of vesicular trafficking, and ion homeostasis, caused similarly high reporter inductions (table S1). Moreover, the UPR up-regulators included several dozen poorly characterized genes, some whose deletion caused reporter induction that rivaled the strongest hits.

The diversity of functions contributing to ER integrity presented a major obstacle in our efforts to understand how these unexpected factors function together to support protein folding in the ER. To overcome this, we explored their functional dependencies by systematically quantifying how the phenotype caused by loss of one gene was modulated by the absence of a second. Systematic analysis of genetic interactions, using growth rate as a phenotype, has been used extensively to determine gene function (9, 18–23). We sought to generalize this strategy by using ER stress as a quantitative phenotype. Accordingly, we quantified GFP reporter levels in over 60,000 strains containing pairwise deletions among 340 of our hits (12).

Genetic interactions illuminate functional relations. Three examples illustrate the utility of the double mutant analysis. First, comparison of the GFP levels in the presence and absence of *IRE1/HAC1* differentiated between the subset of up-regulators whose deletion affected protein folding in the ER (i.e., GFP induction was dependent on the Ire1p/Hac1p pathway) from those, like chromatin architecture genes, that were directly affecting expression of the reporter (Fig. 2A and table S4).

In a second example, UPR levels of pairwise deletions with Δ*die2/alg10*, the enzyme that performs the last step in the synthesis pathway for N-linked glycans, illustrated our ability to define genes acting in a linear pathway (Fig. 2B). Most double mutants showed a typical increase in fluorescence that was dictated solely by the reporter levels of the single mutants. Notably, a specific subset of the double mutants had the same reporter level as the single mutant, indicative of "fully masking" epistatic interactions in which the function of one gene is completely dependent on the presence of a second one. Indeed, the genes that we find to be epistatic to *DIE2* include the full set of factors that act immediately upstream of Die2p in the synthesis of N-linked sugars (16).

The utility of aggravating genetic interactions, in which pairs of deletions lead to exaggerated folding defects, was illustrated in a third example in which we overexpressed the constitutively misfolded and rapidly degraded membrane protein KWS (24) in deletion strains that were hits in our screen (Fig. 2C). KWS degradation is mediated by a well-defined subset of the ERAD machinery, including the E3 ubiquitin ligase Ssm4p/Doa10p and the E2 ubiquitin-conjugating complex Ubc7p and Cue1p (24). The role of these factors in mitigating the stress caused by overexpression of KWS is revealed in our data by the strongly aggravating interaction between their deletions and KWS overexpression. In contrast, other ERAD components, which do not act on KWS, including the Hrd1p/Hrd3p E3 ligase complex (24), show typical reporter levels.
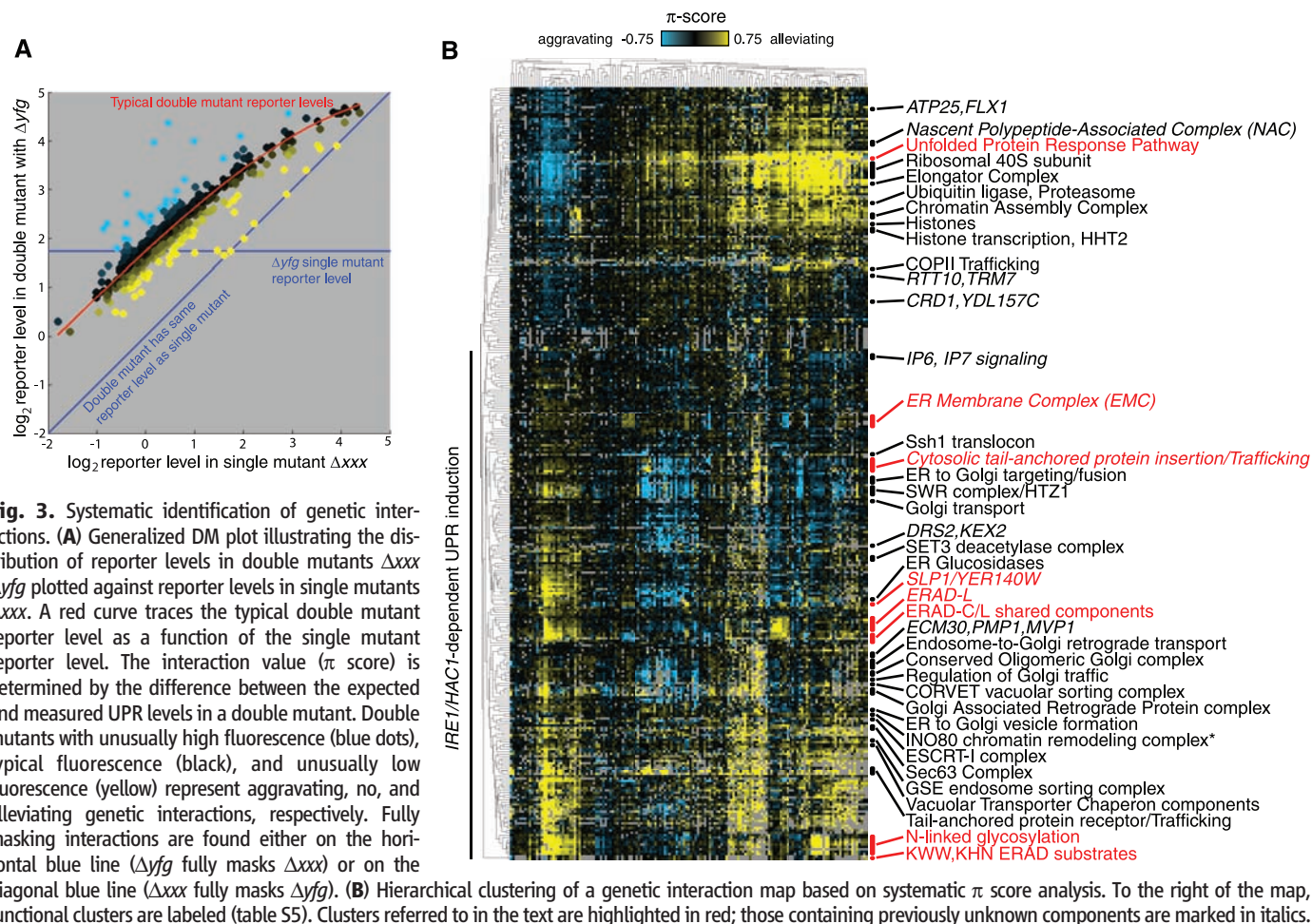

Fig. 3. Systematic identification of genetic interactions. (**A**) Generalized DM plot illustrating the distribution of reporter levels in double mutants Δ*xxx* Δ*yfg* plotted against reporter levels in single mutants Δ*xxx*. A red curve traces the typical double mutant reporter level as a function of the single mutant reporter level. The interaction value (π score) is determined by the difference between the expected and measured UPR levels in a double mutant. Double mutants with unusually high fluorescence (blue dots), typical fluorescence (black), and unusually low fluorescence (yellow) represent aggravating, no, and alleviating genetic interactions, respectively. Fully masking interactions are found either on the horizontal blue line (Δ*yfg* fully masks Δ*xxx*) or on the diagonal blue line (Δ*xxx* fully masks Δ*yfg*). (**B**) Hierarchical clustering of a genetic interaction map based on systematic π score analysis. To the right of the map, functional clusters are labeled (table S5). Clusters referred to in the text are highlighted in red; those containing previously unknown components are marked in italics.

Phenotypic interaction score (π score) quantifies functional relations. Strongly aggravating and fully masking interactions as described above are only a subset of the broader range of possible genetic interactions in which pairs of perturbations lead to a continuum of exacerbated (aggravating) or attenuated folding defects. We sought to quantify these systematically by developing a phenotypic interaction score or "π score" that describes the degree to which a double mutant UPR reporter level differs from that expected from the two single mutant levels. A simple empirical multiplicative model accurately predicted the typical double mutant reporter levels when we accounted for saturation of the reporter [Fig. 3A; see (12)]. The π score for each double mutant was given by the difference between the typical levels expected from the reporter levels of the two single mutants and the measured UPR reporter levels in the double mutant. Thus, negative π scores (exaggerated inductions) represent aggravating interactions, and positive π scores (unusually low inductions) represent alleviating interactions, with the fully masking interactions being a subset of the positive π scores.

Systematic identification of functional groups through phenotypic interaction maps. In growth-based studies, the pattern of genetic interactions of a mutation provides a signature that can be used to group genes by function (20, 21, 25). Analogous hierarchical clustering on the double mutant π scores yielded a map with a high density of precise functional clusters (Fig. 3B and fig. S4). This analysis accurately grouped over 100 of the previously well-characterized genes into 22 functions spanning a wide range of processes (table S5). Among genes whose deletions directly affected the ER folding environment (i.e., caused Ire1p/Hac1p-dependent reporter induction), our map grouped not only the ERAD and glycosylation machinery discussed above but also many other processes, including those in the distal secretory pathway (Fig. 3B). Our map also accurately clustered multiple functions that act downstream of HAC1, including the chromatin assembly complex, core histones, and histone chaperones.

Genetic interactions identify functional hierarchies. Within the functional groups defined above, the specific double mutant phenotypes revealed the extent to which the activities of individual components depended on each other. For example, all of the known components of the ERAD-L machinery needed for disposal of misfolded lumenal proteins (17) formed a tight cluster. The double mutant phenotypes of Δhrd3 revealed the expected full dependence of YOS9, DER1, and USA1 on HRD3

(Fig. 4A) (17). In contrast, only partial epistasis was seen with the E2 Ubc7p and its membrane anchor, Cue1p, consistent with their known roles in other branches of ERAD and the ability of another E2, Ubc1p, to partially substitute in their absence (26). In addition, the clustering analysis suggested that YLR104W is a previously unknown component of ERAD that acts upstream of HRD3 and USA1 (perhaps by delivering a subset of ERAD targets to the Hrd1p ligase) (table S6). Our complete list of genetic interactions, which includes over 500 full masking relations among 213 genes, should provide a resource of functional predictions for the community (table S6). For example, our data suggest that YDR161W is closely functionally related to the nascent polypeptide-associated complex. We also provide a MATLAB script to display double mutant plots for any gene in our data set (12).

Analysis of phenotypic interactions reveals previously unknown pathways important for ER protein folding. By using this systematic approach, we identified a pathway involving a conserved (table S9) multiprotein transmembrane complex. The poorly characterized genes YCL045C, YJR088C, YKL207W, YGL231C, KRE27, and YLL014W all clustered together and showed strongly alleviating interactions among themselves (Fig.
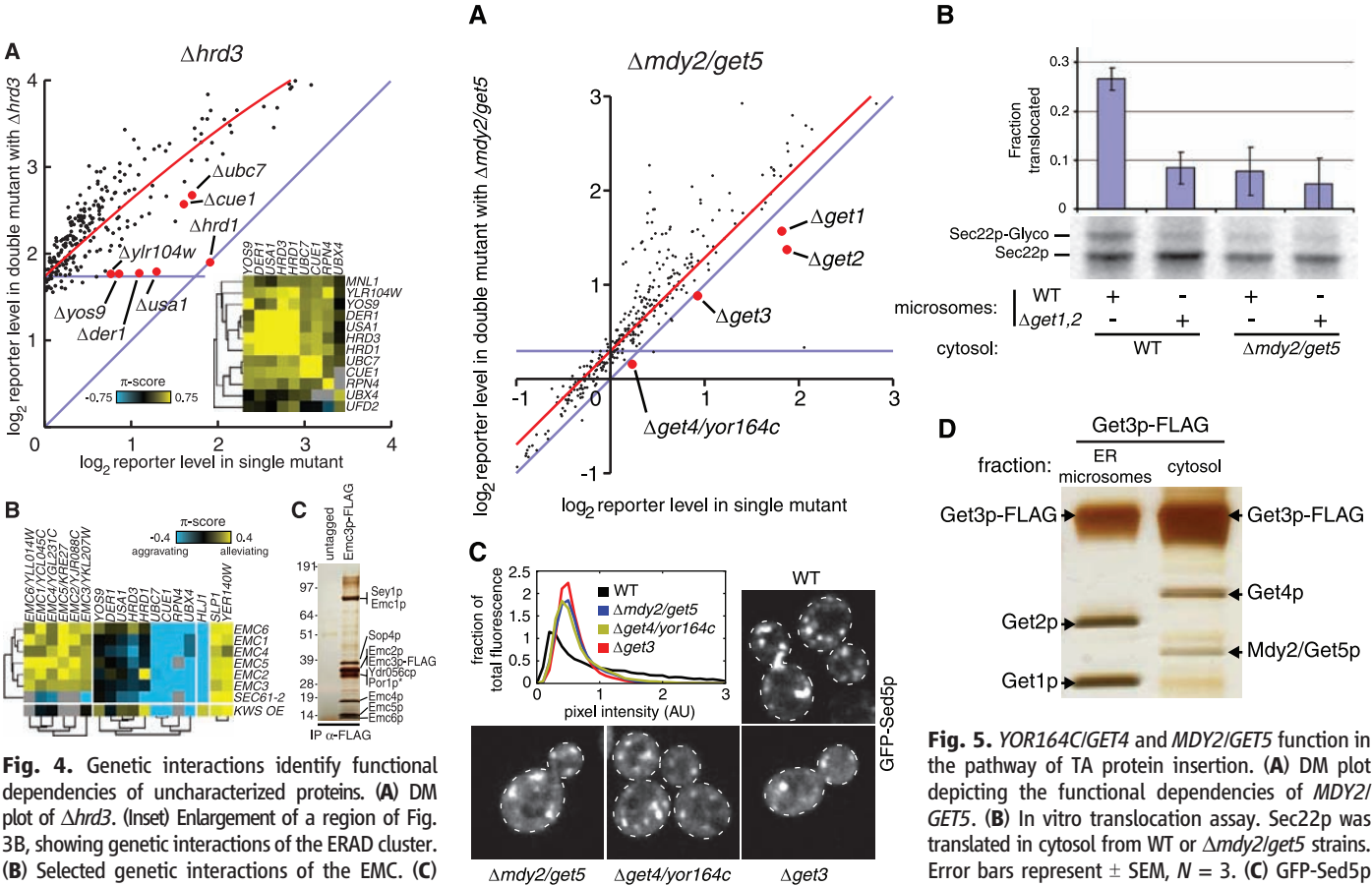

Fig. 4. Genetic interactions identify functional dependencies of uncharacterized proteins. (**A**) DM plot of Δhrd3. (Inset) Enlargement of a region of Fig. 3B, showing genetic interactions of the ERAD cluster. (**B**) Selected genetic interactions of the EMC. (**C**) SDS–polyacrylamide gel electrophoresis analysis of immunoprecipitation of Emc3p-FLAG and associated proteins; protein identities were determined by mass spectrometry. The specificity of the Por1p interaction has not been evaluated.

Fig. 5. YOR164C/GET4 and MDY2/GET5 function in the pathway of TA protein insertion. (**A**) DM plot depicting the functional dependencies of MDY2/GET5. (**B**) In vitro translocation assay. Sec22p was translated in cytosol from WT or Δmdy2/get5 strains. Error bars represent ± SEM, N = 3. (**C**) GFP-Sed5p localization defect in Δget3, Δget4, and Δmdy2/get5 strains. The images of at least 20 cells per strain with similar average fluorescence were quantified to determine the distribution of each strain's total fluorescence across pixels of different intensities. (**D**) Silver stain of immunoprecipitation of Get3-FLAGp from ER microsomes and cytosol; protein identities were determined by mass spectrometry.

4B), a signature of factors that cooperate to carry out a single function (21). Immunoprecipitation of FLAG-tagged Ykl207wp revealed that proteins encoded by these genes form an apparently stoichiometric complex (Fig. 4C). Accordingly we termed this the ER membrane protein complex (EMC) and named the genes from this cluster *EMC1* through *EMC6*. Although the precise biochemical roles of the EMC will have to wait for future studies, our data suggest that loss of the EMC leads to accumulation of misfolded membrane proteins: The pattern of genetic interactions of strains deleted for EMC members most closely resembled that seen in a strain overexpressing the misfolded transmembrane protein Sec61-2p (a mutated form of the Sec61 translocon) (27) and is similar to the pattern of a strain overexpressing the misfolded transmembrane protein KWS (24). This shared pattern includes strong aggravating interactions with Δ*ubc7* and Δ*cue1*, whose gene products are known to be involved in elimination of misfolded membrane proteins (17), but minimal interactions with other ERAD components.

A second cluster containing two conserved yet uncharacterized proteins (Yer140wp and Slp1p) show robust alleviating interactions with EMC components (Fig. 4B), as well as with each other. In support of a functional link between Yer140wp and Slp1p, these two proteins are suggested to be in a physical complex (28). The finding of two conserved protein complexes that are functionally dependent on each other underscores the value of this genetic data in identifying uncharacterized pathways required for ER folding.

Genetic interactions identify components of the tail-anchored protein biogenesis machinery. As a final example, we focused on Yor164c/Get4p and Mdy2/Tma24/Get5p because our analysis implicated them in tail-anchored (TA) protein biogenesis. TA proteins are an important class of transmembrane proteins, which includes soluble *N*-ethylmaleimide–sensitive factor attachment protein receptor (SNARE) trafficking factors (29, 30). TA proteins have a single C-terminal transmembrane domain, which is inserted into the ER membrane through the action of the recently discovered GET pathway: the Get3p/Arr4p adenosine triphosphatase (and its mammalian homolog Asna1/TRC40) binds newly synthesized TA proteins and brings them to the ER via the ER membrane receptor complex formed by Get1p/Mdm39p and Get2p/Hur2p/Rmd7p (31–33). Our double mutant analysis pointed to a role of Yor164c/Get4p and its physical interaction partner, Mdy2p/Get5p (34), in the GET pathway because Δ*get4* and Δ*mdy2/get5* tightly clustered with Δ*get3* (fig. S5). Additionally, loss of *GET3* fully masked the effect of Δ*get4* and Δ*mdy2/get5* (Fig. 5A). Moreover, these deletions partially suppressed the UPR induction of Δ*get1* and Δ*get2*, a phenomenon previously seen with other phenotypes for Δ*get3* (32).

Several observations support a role for *GET4* and *MDY2*/*GET5* in TA protein biogenesis. First, cytosolic extracts from strains lacking Mdy2p/Get5p had a defect in insertion of the model TA substrate Sec22p into ER microsomes (Fig. 5B). Second, several of the in vivo phenotypes characteristic of loss of GET members are also observed in Δ*get4* and Δ*mdy2/get5* strains. These include a highly significant ($P < 10^{-30}$, Mann-Whitney U) relocalization of TA protein GFP-Sed5p from punctate Golgi structures to a more diffuse pattern (Fig. 5C and fig. S7) (12) as well as mislocalization of the peroxisomal TA protein, GFP-Pex15p, to mitochondria (fig. S8) (32). Consistent with a defect in Sed5 biogenesis, loss of Get4p or Mdy2p/Get5p led to secretion of HDEL proteins, a phenotype that is seen in other GET deletion strains (fig. S9). Third, immunoprecipitation revealed that Get4p and Mdy2p/Get5p bind Get3p in the cytosol (Fig. 5D). Mdy2p/Get5p also colocalized with Get3p and TA proteins to punctate protein aggregates that form in Δ*get1* strains (32) (figs. S10 and S11). Localization of Get3 to these puncta is dependent on Get4p and Mdy2p/Get5p but not vice versa (figs. S10 to S12), suggesting that Get4p and Mdy2p/Get5p help deliver TA proteins to Get3p in the cytosol for trafficking to the ER membrane. Interestingly, Get4p and Mdy2p/Get5p have been suggested to be peripherally associated with ribosomes (34), where they could potentially capture nascent TA proteins. Thus, whereas Get4p and Mdy2p/Get5p are localized outside of the secretory pathway and initially may have appeared to be false positives, our double mutant analysis revealed how they affect ER protein folding.

Perspective. Our work reveals the range of processes that make the ER a robust folding compartment and yields both a list of components and a blueprint for their functional interdependence. These factors include a wide range of activities such as chaperones, glycosylation enzymes, and ERAD components as well as trafficking pathways, transcriptional regulatory networks, modulators of lipid and ion composition, and vacuolar function. The diversity of activities found supports and extends the recent view in which ER protein folding homeostasis (proteostasis) emerges from the dynamic interplay between folding, degradation, and export processes (35, 36). From a practical perspective, our studies provide a rational starting point for efforts to modulate the ER folding capacity to intervene in disease (36).

More broadly, dissecting complex cellular processes represents a major challenge in cell biology. Deletion libraries and RNA interference (RNAi) approaches now make it possible to identify important factors rapidly (37). But this in turn creates a bottleneck in their functional characterization, which classically requires specialized gene-by-gene follow-up studies. Our approach in effect allows hundreds of different secondary screens to be carried out in parallel to explore systematically the functional interdependencies of hits, thus providing a foundation for focused mechanistic investigations. Given the large number of potential ways of creating proximal reporters for different aspects of biology, our strategy for generalizing systematic quantitative genetic analysis should be broadly applicable to other processes and organisms, including mammals, through the use of double RNAi treatments.

References and Notes

1. J. H. Lin, P. Walter, T. S. Yen, *Annu. Rev. Pathol.* **3**, 399 (2008).
2. D. Scheuner, R. J. Kaufman, *Endocr. Rev.* **29**, 317 (2008).
3. D. N. Hebert, M. Molinari, *Physiol. Rev.* **87**, 1377 (2007).
4. E. S. Trombetta, A. J. Parodi, *Annu. Rev. Cell Dev. Biol.* **19**, 649 (2003).
5. D. Ron, P. Walter, *Nat. Rev. Mol. Cell Biol.* **8**, 519 (2007).
6. R. Casagrande et al., *Mol. Cell* **5**, 729 (2000).
7. K. J. Travers et al., *Cell* **101**, 249 (2000).
8. M. G. Pollard, K. J. Travers, J. S. Weissman, *Mol. Cell* **1**, 171 (1998).
9. A. H. Y. Tong et al., *Science* **294**, 2364 (2001).
10. G. Giaever et al., *Nature* **418**, 387 (2002).
11. J. R. Newman et al., *Nature* **441**, 840 (2006).
12. Materials and methods are available as supporting material on *Science* Online.
13. E. A. Winzeler et al., *Science* **285**, 901 (1999).
14. W. K. Huh et al., *Nature* **425**, 686 (2003).
15. B. Bukau, J. Weissman, A. Horwich, *Cell* **125**, 443 (2006).
16. A. Helenius, M. Aebi, *Annu. Rev. Biochem.* **73**, 1019 (2004).
17. K. Nakatsukasa, J. L. Brodsky, *Traffic* **9**, 861 (2008).
18. L. Decourty et al., *Proc. Natl. Acad. Sci. U.S.A.* **105**, 5821 (2008).
19. H. S. Girgis, Y. Liu, W. S. Ryu, S. Tavazoie, *PLoS Genet.* **3**, 1644 (2007).
20. X. Pan et al., *Cell* **124**, 1069 (2006).
21. M. Schuldiner et al., *Cell* **123**, 507 (2005).
22. D. Segre, A. Deluna, G. M. Church, R. Kishony, *Nat. Genet.* **37**, 77 (2005).
23. R. P. St Onge et al., *Nat. Genet.* **39**, 199 (2007).
24. S. Vashist, D. T. Ng, *J. Cell Biol.* **165**, 41 (2004).
25. A. H. Y. Tong et al., *Science* **303**, 808 (2004).
26. R. Friedlander, E. Jarosch, J. Urban, C. Volkwein, T. Sommer, *Nat. Cell Biol.* **2**, 379 (2000).
27. T. Sommer, S. Jentsch, *Nature* **365**, 176 (1993).
28. S. R. Collins et al., *Mol. Cell. Proteomics* **6**, 439 (2007).
29. L. Burri, T. Lithgow, *Traffic* **5**, 45 (2004).
30. N. Borgese, S. Brambillasca, P. Soffientini, M. Yabal, M. Makarow, *Biochem. Soc. Trans.* **31**, 1238 (2003).
31. V. Favaloro, M. Spasic, B. Schwappach, B. Dobberstein, *J. Cell Sci.* **121**, 1832 (2008).
32. M. Schuldiner et al., *Cell* **134**, 634 (2008).
33. S. Stefanovic, R. S. Hegde, *Cell* **128**, 1147 (2007).
34. T. C. Fleischer, C. M. Weaver, K. J. McAfee, J. L. Jennings, A. J. Link, *Genes Dev.* **20**, 1294 (2006).
35. W. E. Balch, R. I. Morimoto, A. Dillin, J. W. Kelly, *Science* **319**, 916 (2008).
36. T. W. Mu et al., *Cell* **134**, 769 (2008).
37. M. Boutros, J. Ahringer, *Nat. Rev. Genet.* **9**, 554 (2008).
38. We thank C.-S. Chin for flow cytometry software development; C. Boone, D. Breslow, N. Krogan, D. Ng, and C. Wang for reagents; K. Thorn for microscopy assistance; S. Zhou, D. King, G. Cagney, and N. Krogan for mass spectrometry analyses; J. Metz, P. Nittler, A. Carroll, J. Hill, J. Ihmels, S. Wang, and C. Chu for technical help; R. Andino, T. Aragon, A. Battle, N. Bradshaw, J. DeRisi, N. Friedman, J. Hollien, J. Newman, D. Koller, R. Kupferman, H. Madhani, L. Osherovich, F. Papa, and members of the Weissman, Walter, and Schwappach labs for stimulating discussion; B. Toyama for graphics; and M. Bassik, D. Breslow, O. Brandman, S. Churchman, and S. Neher for comments on the manuscript. This work was supported by the Howard Hughes Medical Institute (J.S.W. and P.W.), the NSF (M.C.J. and E.M.Q.), the International Human Frontier Science Program (M.S. and J.W.), an NIH K99/R00 award (M.S.), a European Molecular Biology Organization long-term fellowship (J.W.), the Deutsche Forschungsgemeinschaft (V.S.), and the Wellcome Trust (B.S.).

Editor's Summary

Article Tools	Visit the online version of this article to access the personalization and article tools: http://science.sciencemag.org/content/323/5922/1693
Permissions	Obtain information about reproducing this article: http://www.sciencemag.org/about/permissions.dtl